Electronic Supplementary Information

A tripodal imine derived Fe(III) complex for fluorescence recognition of Mg(II) via green emission: crystal structure, photo-physical interactions and DFT studies

Jayanta Das, Sangita Maji, Prasenjit Mandal, Subhasis Ghosh and Debasis Das*

Department of Chemistry, The University of Burdwan, Burdwan, 713104, W.B., India

Correspondence: D Das: ddas100in@yahoo.com

1. Experimental

Apparatus and reagents

Details about reagents and apparatus used in this report have been described here. HEPES buffer, tris-(2-aminoethyl)amine, 3-ethoxysalicylaldehyde, $FeSO_4.7H_2O$, $MgCl_2.6H_2O$ are purchased from Merck (India). Solvents used are of spectroscopic grade and chemicals are of analytical reagent grade. UV-Vis. spectra are recorded using Shimadzu Multi Spec 2450 spectrophotometer. Prestige 21 CE Shimadzu FTIR spectrophotometer is used for recording FTIR spectra. ^{1}H NMR spectra are recorded by Bruker Advance 400 (400 MHz) spectrometer. Chemical shift values are reported in terms of parts per million (ppm) and tetramethylsilane is used as reference. Multiplicity was depicted as: s (singlet), d (doublet), t (triplet), q (quartet), m (multiplet). Coupling constants are reported in Hertz (Hz). High resolution mass spectra were obtained on a Xevo G2S/Q-Toff. microTM spectrometer. Elemental analyses have been performed on a Perkin Elmer 2400 CHN analyzer. Hitachi F-4500 spectrofluorimeter is used to record steady state emission and excitation spectra. Time-resolved fluorescence lifetime data are collected using time-correlated single-photon counting spectrometer (IBH, UK, λ_{ex}, 348 nm), attached to an MCP-PMT detector. The data are plotted by modern technique using a software IBH DAS 6.2 data analysis. Measurement of solution pH have been performed using Systronics digital pH meter (model 335).

2. General method of UV-Vis and fluorescence titration

A cell of 1 cm path length is used for absorption and emission studies. To measure UV-Vis. and fluorescence data, stock solution of **[Fe(III)-TNESAL]** is prepared (20 μM) in DMF/H_2O (3/1, v/v) HEPES (10 mM) buffer. Working solutions of **[Fe(III)-TNESAL]** and Mg^{2+} (from $MgCl_2$) are prepared from their respective stock solutions. Fluorescence data are collected using 5 nm x 5 nm slit width.

2. **Job's plot from fluorescence experiment**

A series of solutions have been prepared in such a way that the total concentration of Mg^{2+} and [**Fe(III)-TNESAL]** remain constant (20 μM) in all the sets. The mole fraction (X) of [**Fe(III)-TNESAL]** is varied from 0.1 to 0.9. The emission intensity at 488 nm is plotted against mole fraction of [**Fe(III)-TNESAL]** in solution.

4. Calculation of detection limit

The detection limit (DL) is determined from the following equation:

$$DL = \frac{3\sigma}{S}$$

where σ is the standard deviation of the blank solution, S is the slope of the calibration curve. S = 403.2927

5. Determination of binding constant:

The replacement binding constant of [**Fe(III)-TNESAL]** for Mg^{2+} is determined using the following equation.

$$\frac{F_{max} - F_{min}}{F_X - F_{min}} = 1 + \frac{1}{K[C]^n}$$

Where $\mathbf{F_{min}}$, $\mathbf{F_x}$, and $\mathbf{F_{max}}$ are the emission intensities of **Fe(III)-TNESAL** in absence of analyte, at an intermediate analyte concentration, and at a concentration of complete interaction with

analyte respectively. **K** is the binding constant, **C** is the concentration of analyte and **n** is the number of analyte bound per probe molecule (here, **n** = 1). The value of **K** is calculated from the slope of the plot.

6. Calculation of quantum yield

Fluorescence quantum yield of the compound relative to anthracene, whose quantum yield is known (**Φ = 0.27**) in ethanol medium, is measured using the following equation.

$$\Phi_s = \Phi_r \frac{A_r F_s \eta_s^2}{A_s F_r \eta_r^2}$$

F_s and F_r are relative integrated fluorescence intensities of sample and reference solution, η_s and η_r are the refractive index of corresponding solvents, A_s and A_r are their absorbance at the same excitation wavelength (λ_{ex} = 348 nm for DMF-H_2O media).

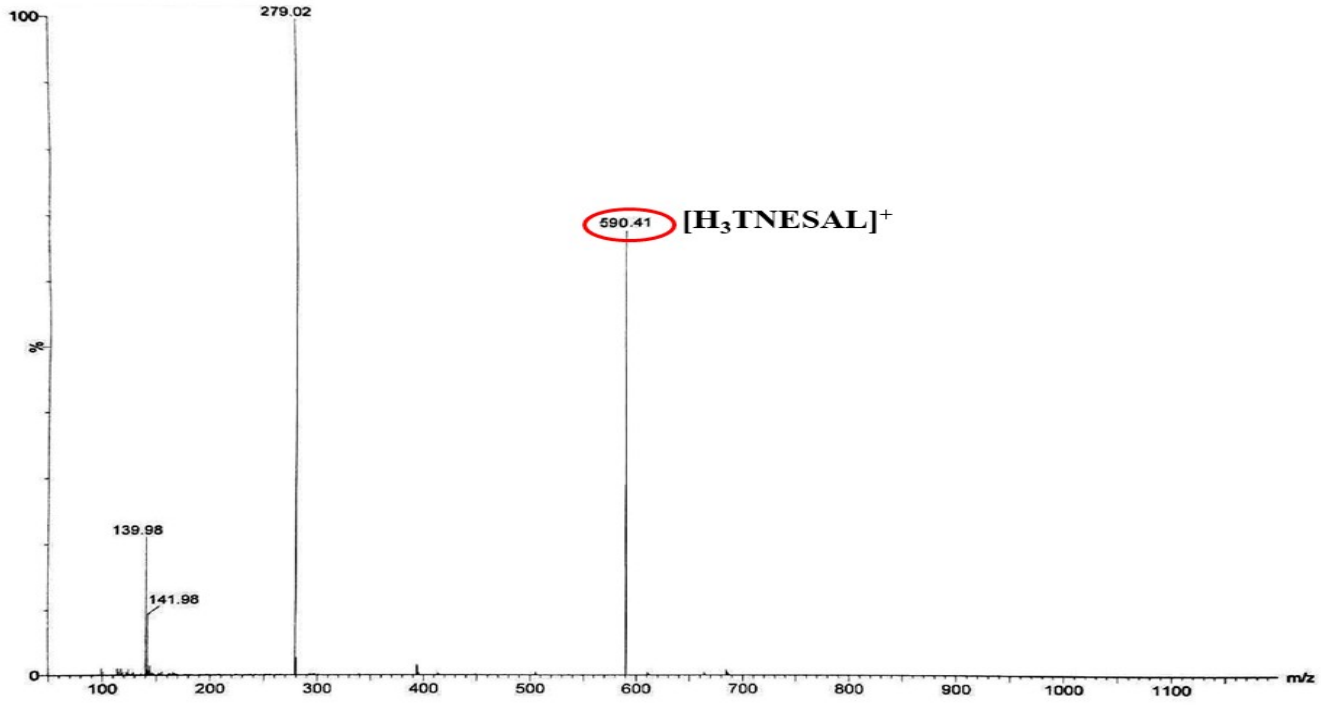

Fig. S1 Mass spectrum of H_3TNESAL

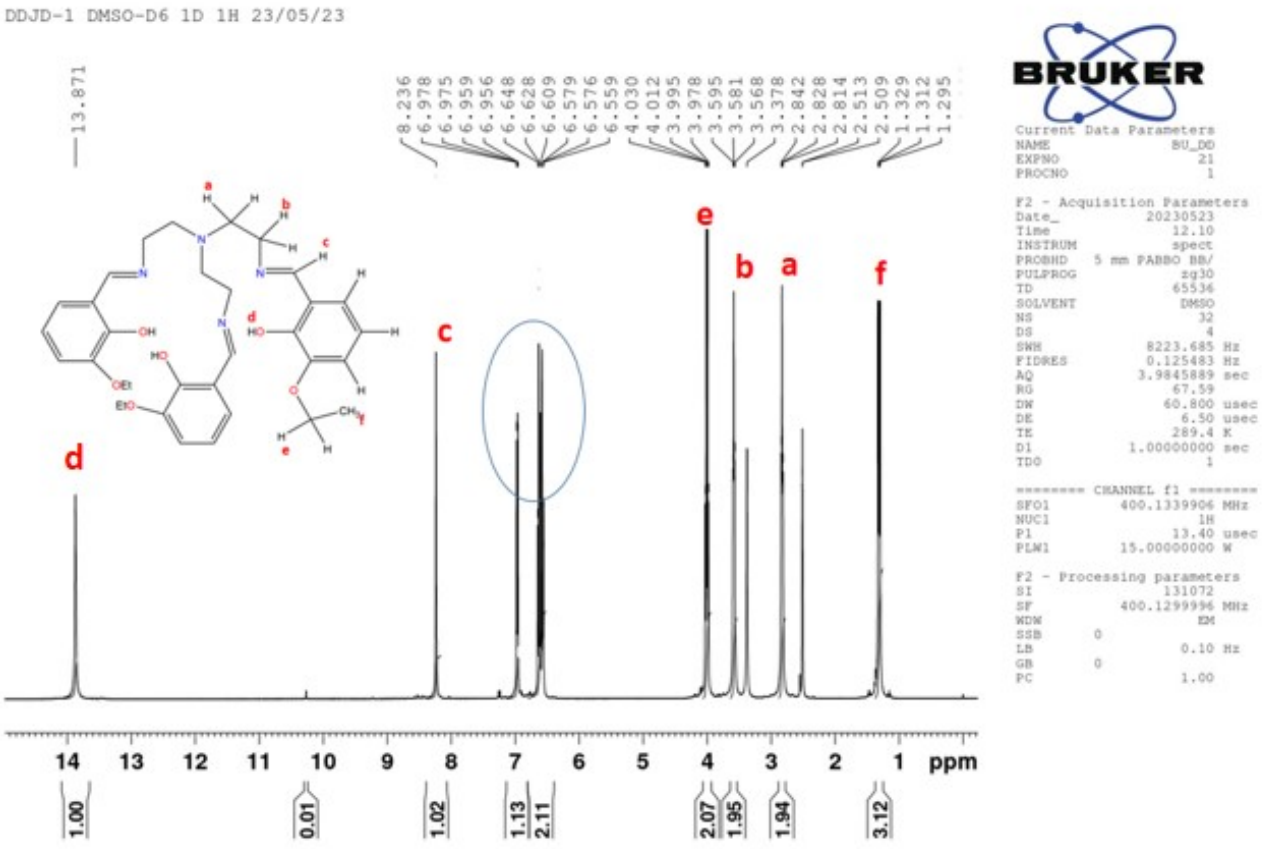

Fig. S2a ^{1}H NMR spectrum of **H_3TNESAL** in DMSO-d_6

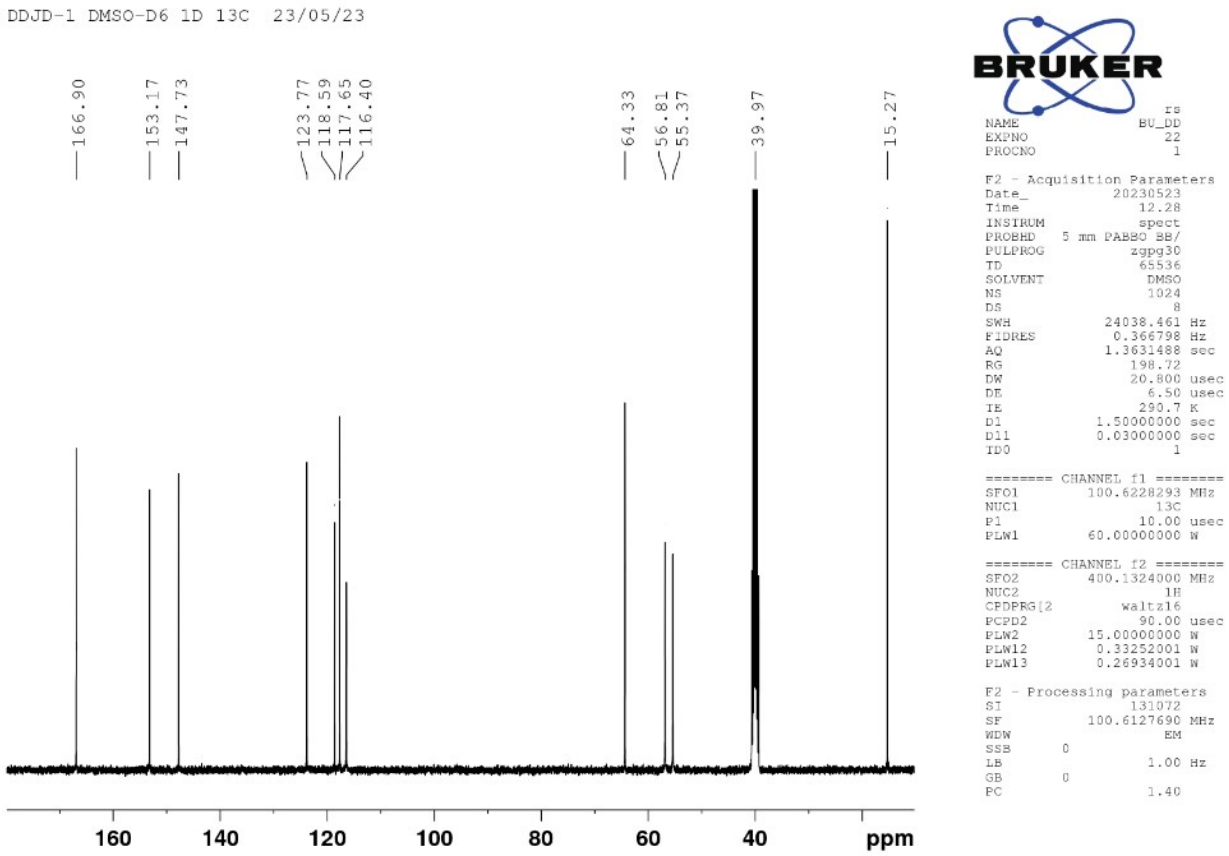

Fig. S2b ^{13}C NMR spectrum of **H_3TNESAL** in DMSO-d_6

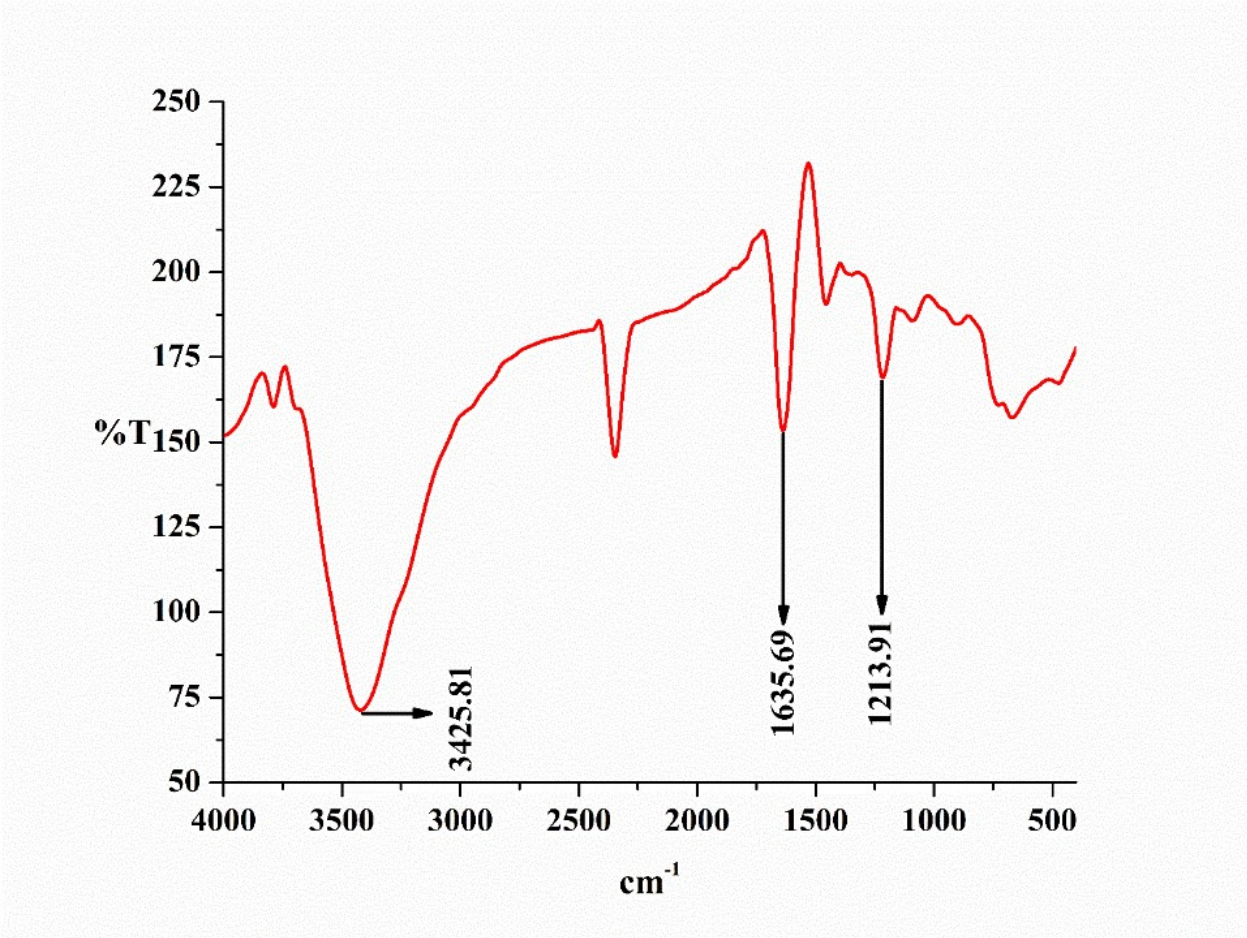

Fig. S3 FTIR spectrum of **H_3TNESAL**

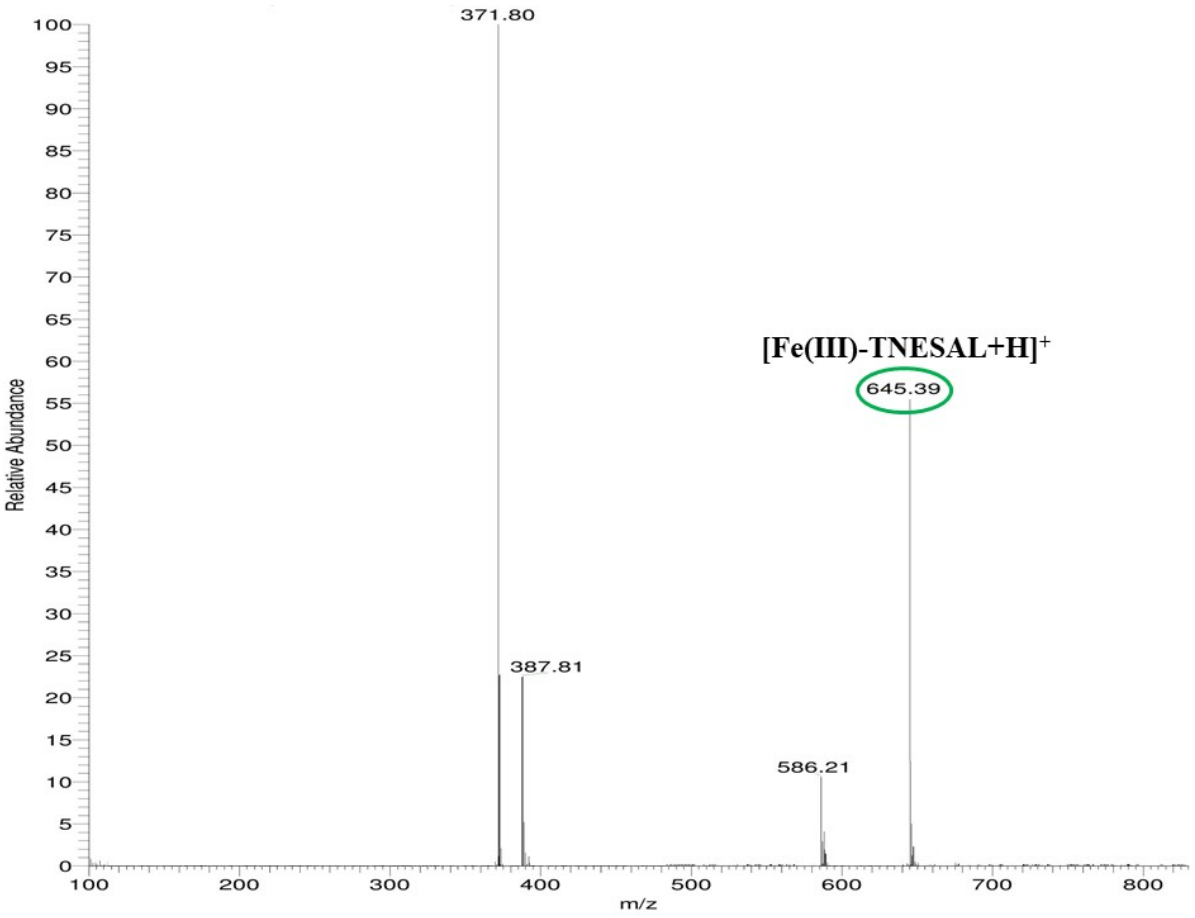

Fig. S4 Mass spectrum of **[Fe(III)-TNESAL]** complex

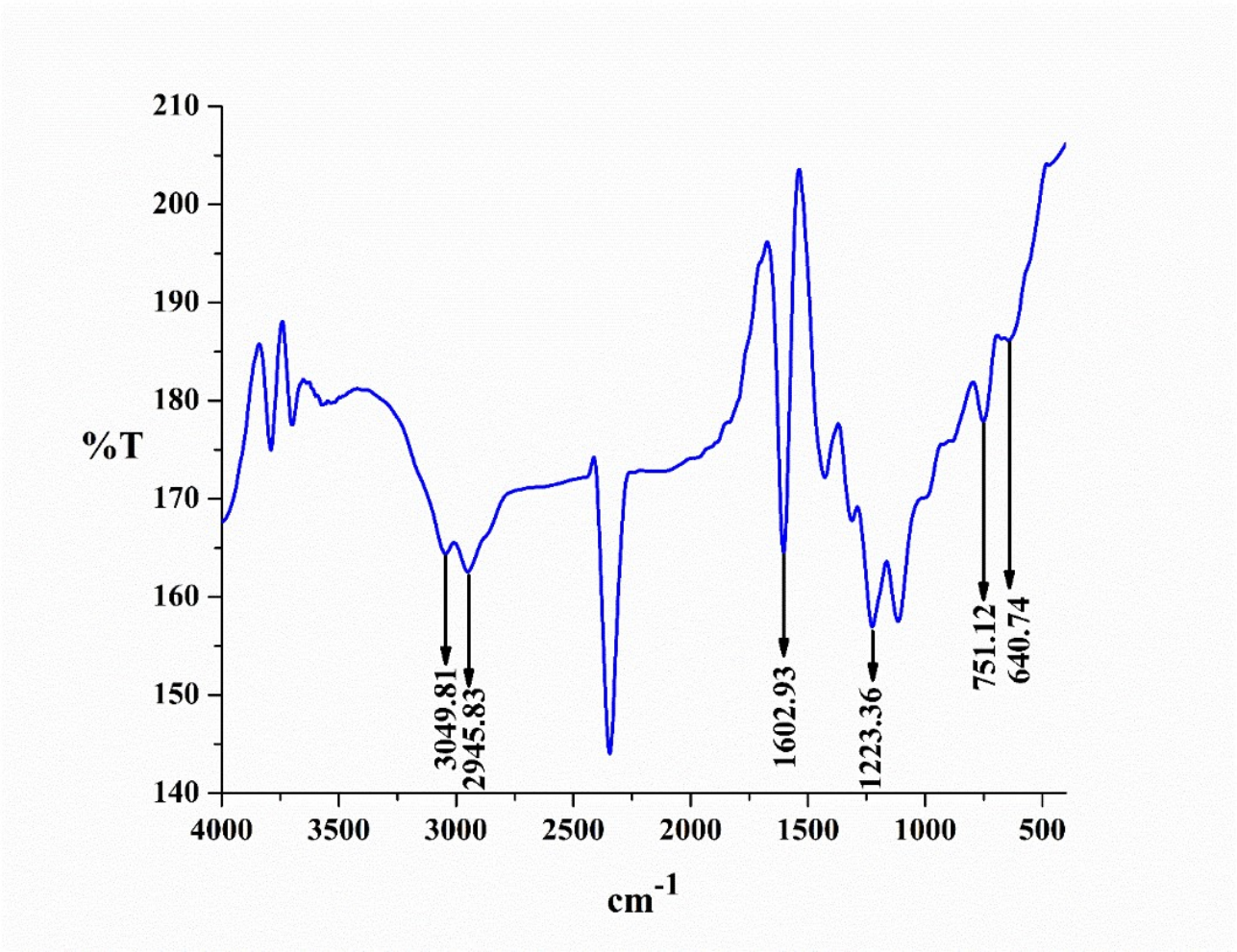

Fig. S5 FTIR spectrum of [**Fe(III)-TNESAL]** complex

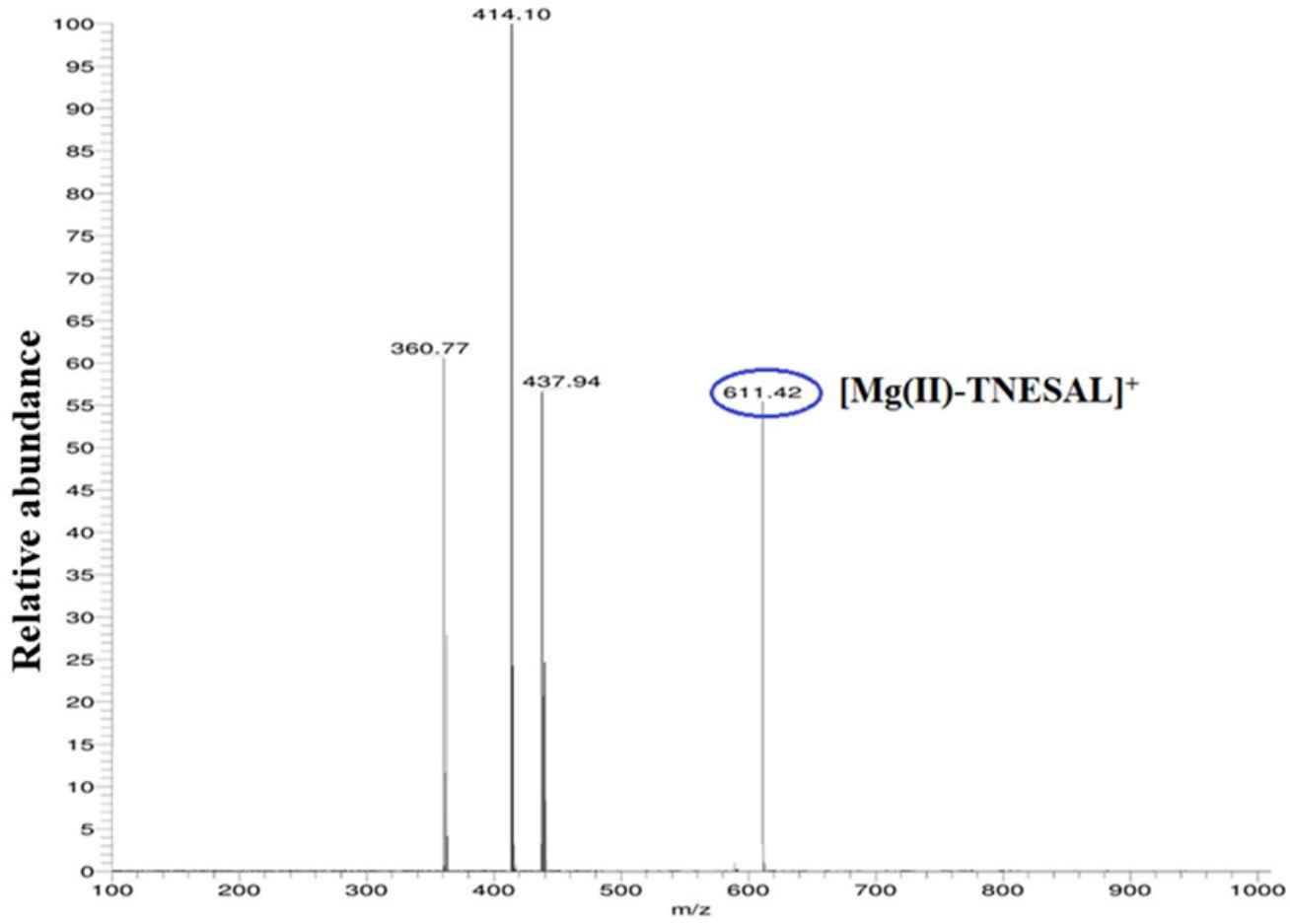

Fig. S6a Mass spectrum of [**Mg(II)-TNESAL]** complex

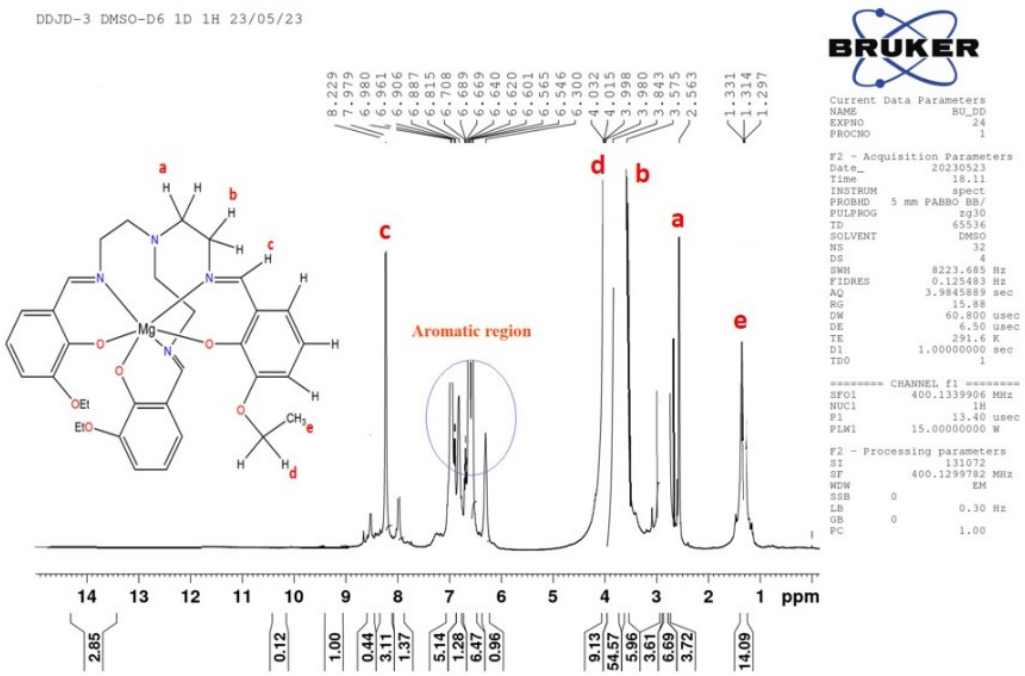

Fig. S6b ^{1}H NMR spectrum of **[Mg(II)-TNESAL]** in DMSO-d_6

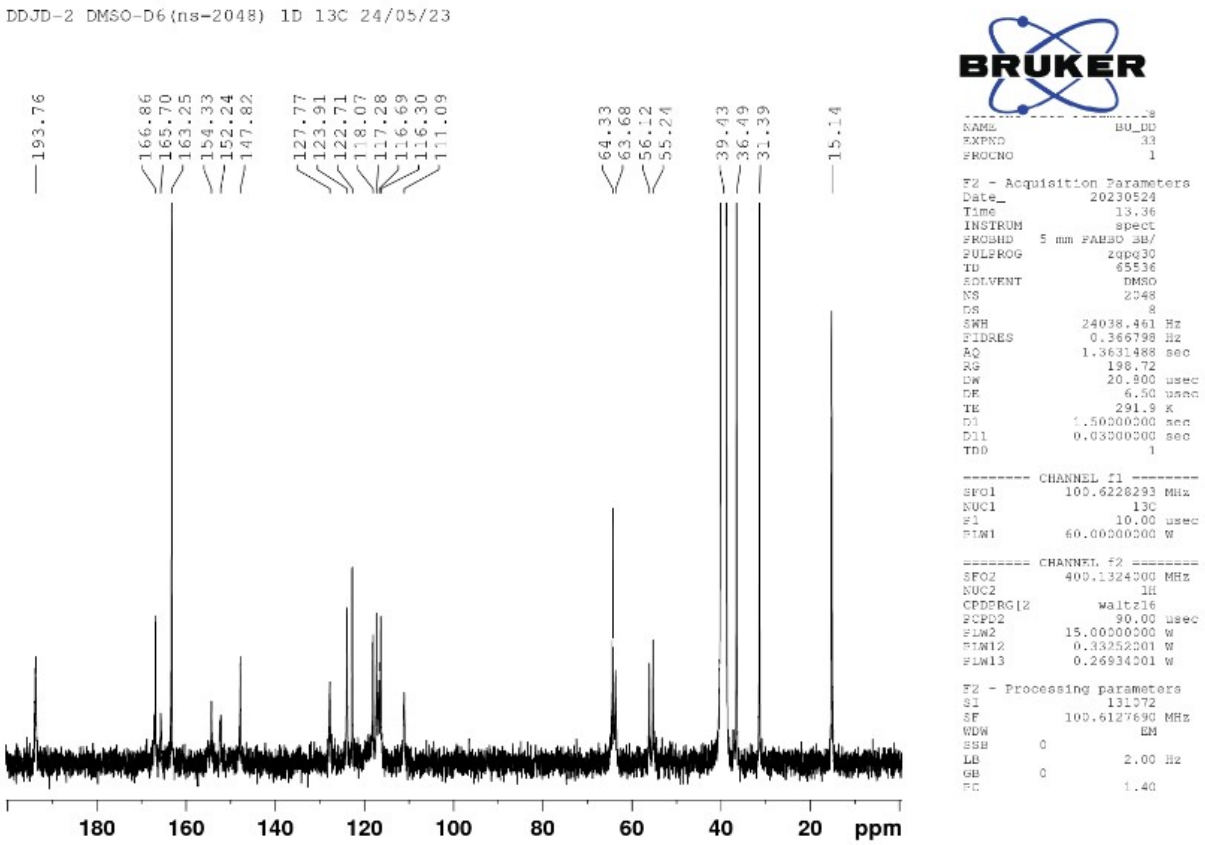

Fig. S6c ^{13}C NMR spectrum of **[Mg(II)-TNESAL]** in DMSO-d_6

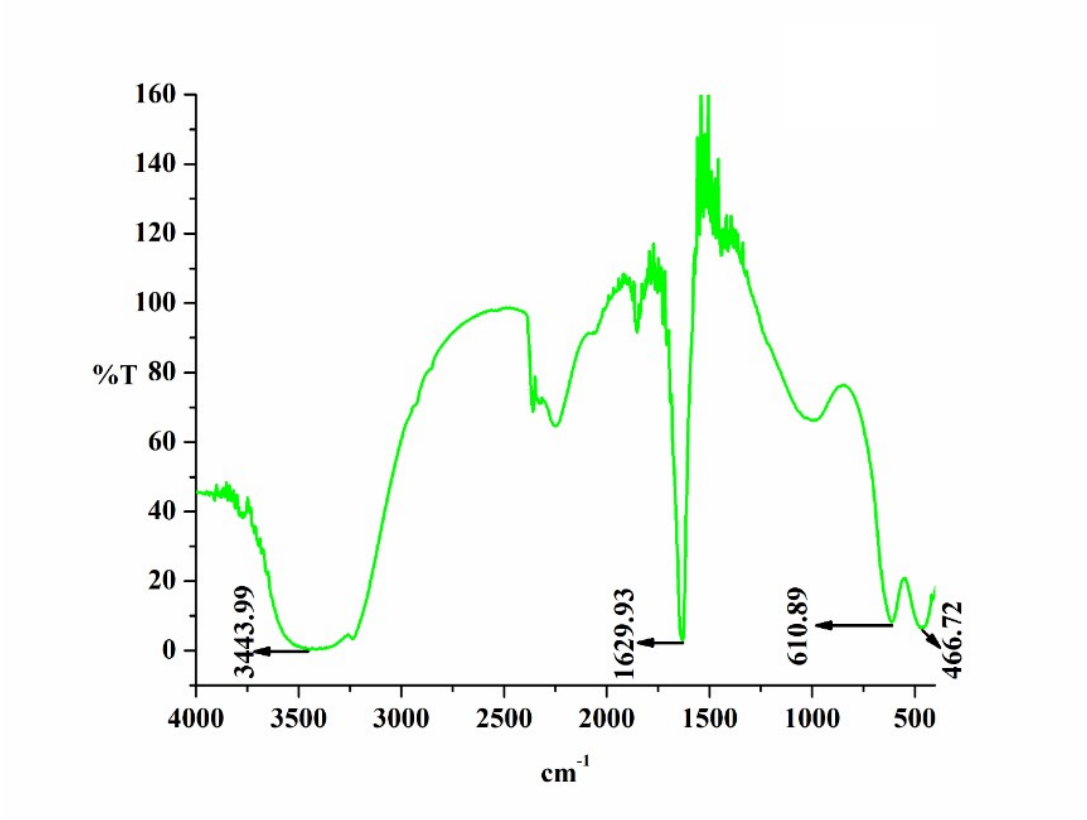

Fig. S7 FTIR spectrum of [**Mg(II)-TNESAL]** complex

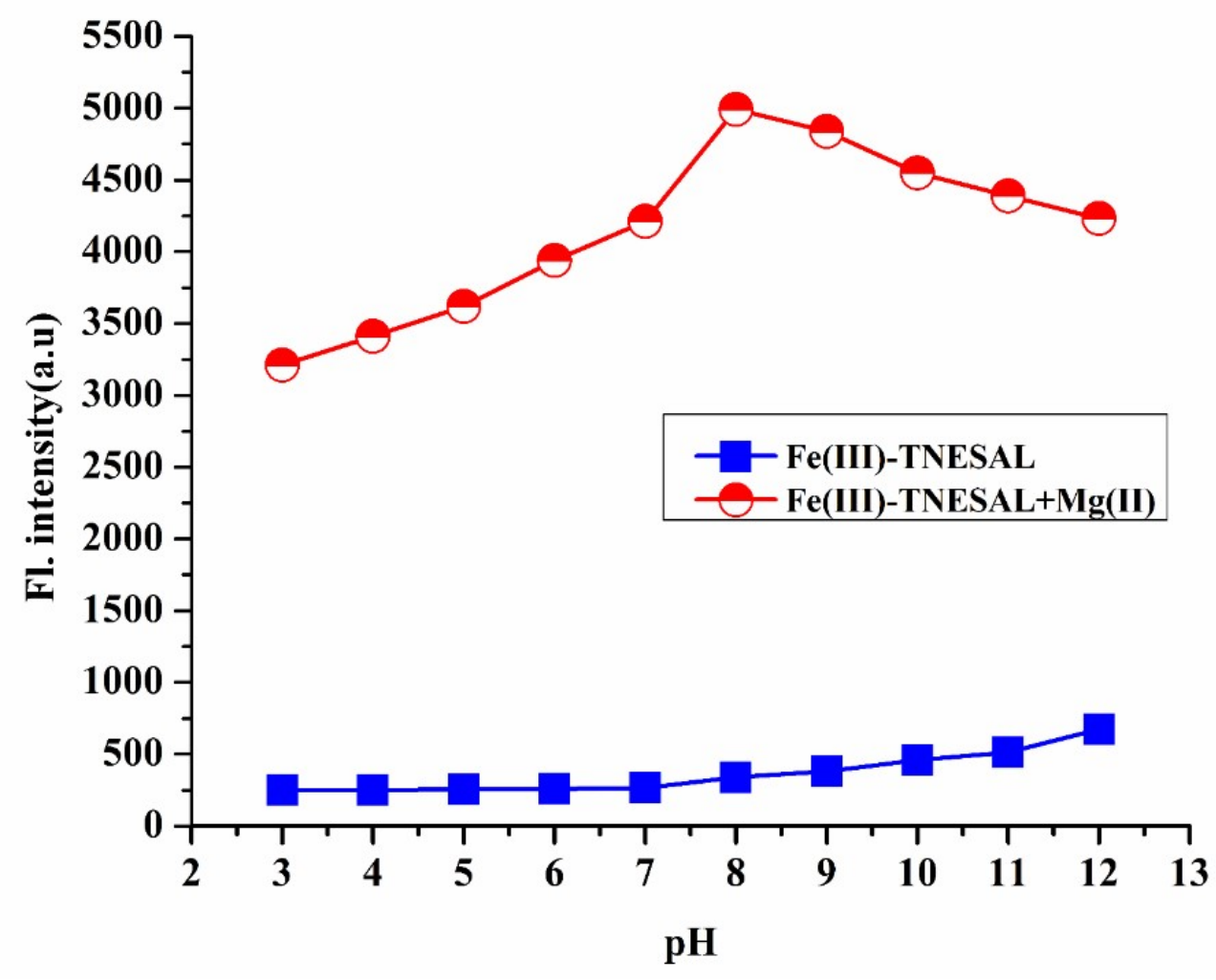

Fig.S8 Influence of pH on the emission profile of **[Fe(III)-TNESAL]** (20 μM, DMF/ H_2O, 3:1, v/v, λ_{em}, 488 nm) in presence and absence of Mg^{2+}

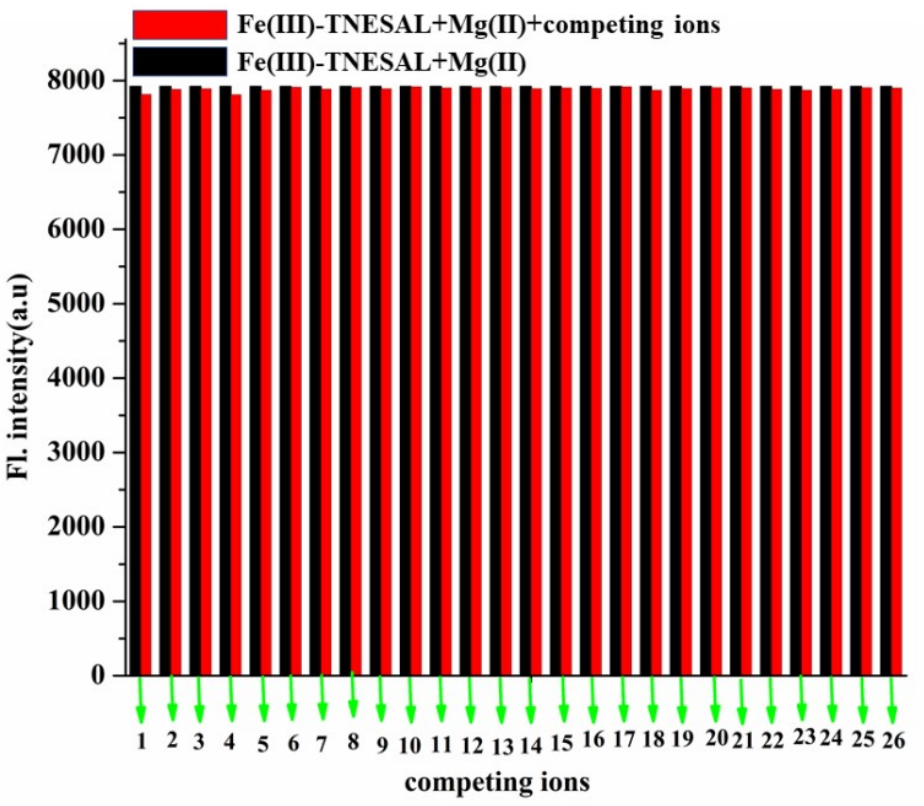

Fig.S9 Emission intensity of **[Fe(III)-TNESAL]** (20 μM) at 488 nm in presence of different ions (200 μM) such as 1: V^{3+}, 2: Cr^{3+}, 3: Mn^{2+}, 4: Co^{2+}, 5: Ni^{2+}, 6: Na^{+}, 7: K^{+}, 8: Li^{+}, 9: Cl^{-}, 10: Ca^{2+}, 11: Al^{3+}, 12: Sn^{2+}, 13: Pd^{2+}, 14: Pt^{4+}, 15: Br^{-}, 16: I^{-}, 17: SO_4^{2-} 18: PO_4^{3-}, 19: Fe^{3+}, 20: Fe^{2+}, 21: Hg^{2+}, 22: Pb^{2+}, 23: Cd^{2+}, 24: Zn^{2+}, 25: Cu^{2+}, 26: Ag^{+} in DMF/ H_2O (3/1, v/v, 20 μM, λ_{ex}, 348 nm)

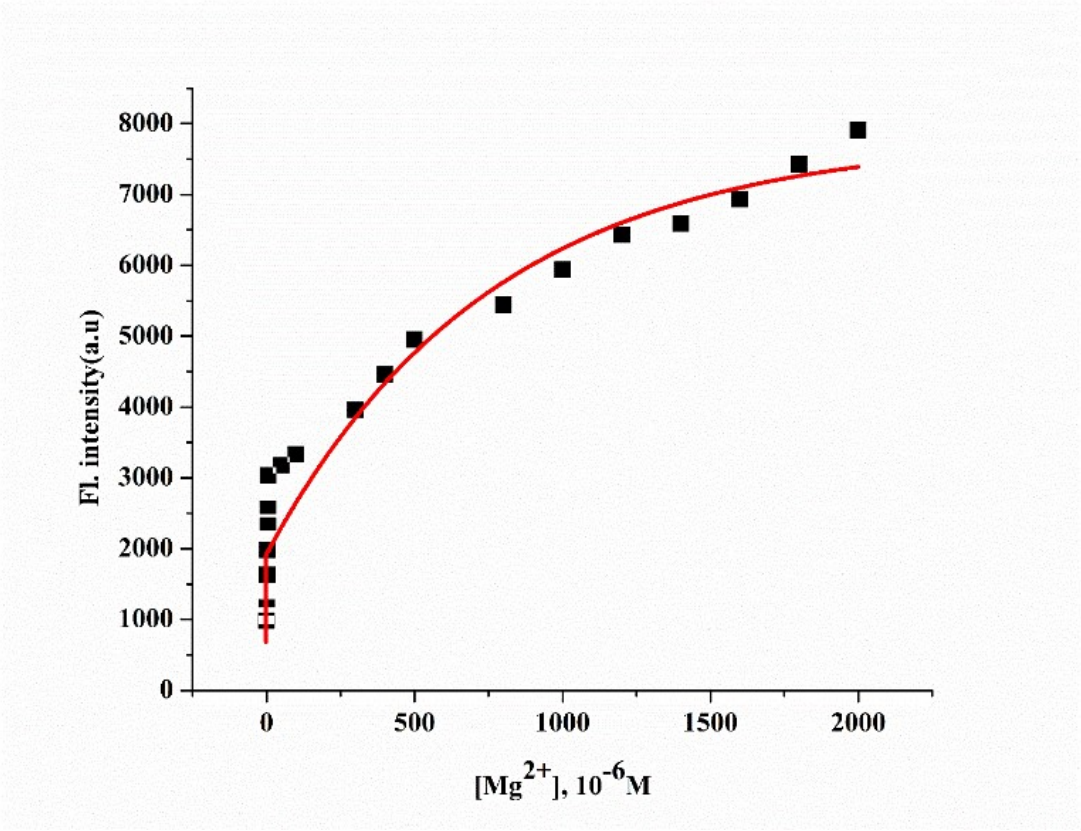

Fig.S10 Plot of emission intensities of **[Fe(III)-TNESAL]** (20 μM) as a function of added Mg^{2+} (0-200 μM) at 488 nm (λ_{ex}, 348 nm).

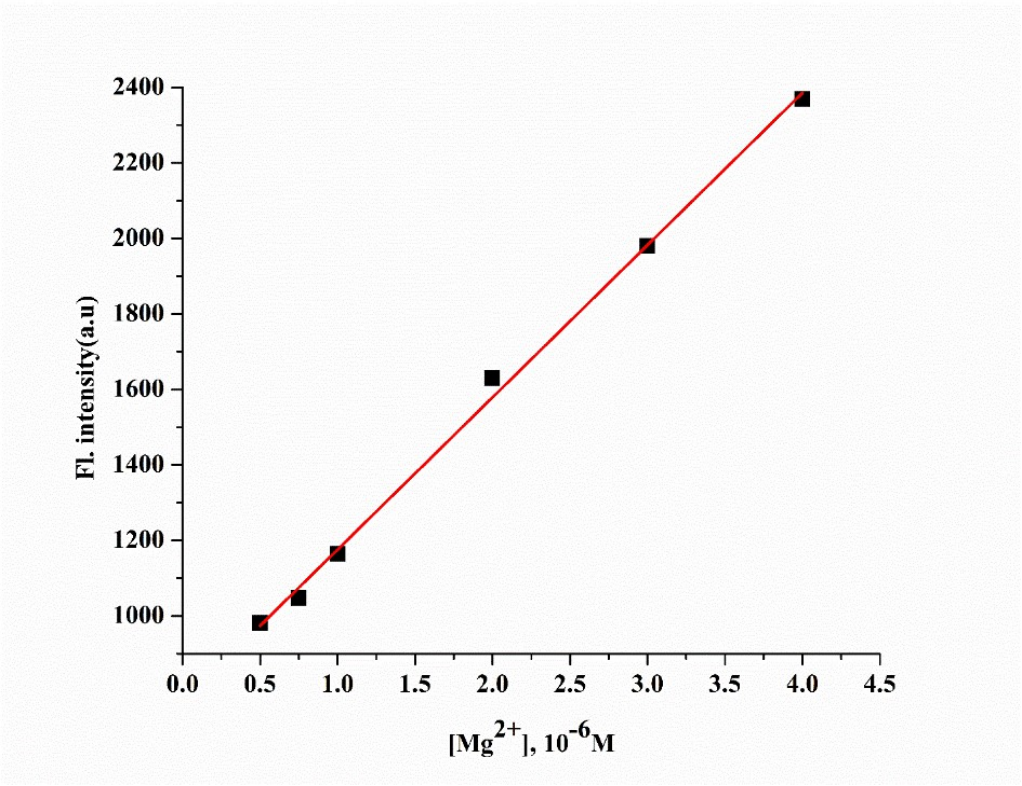

Fig. S11 Linear region of Fig.**S10**

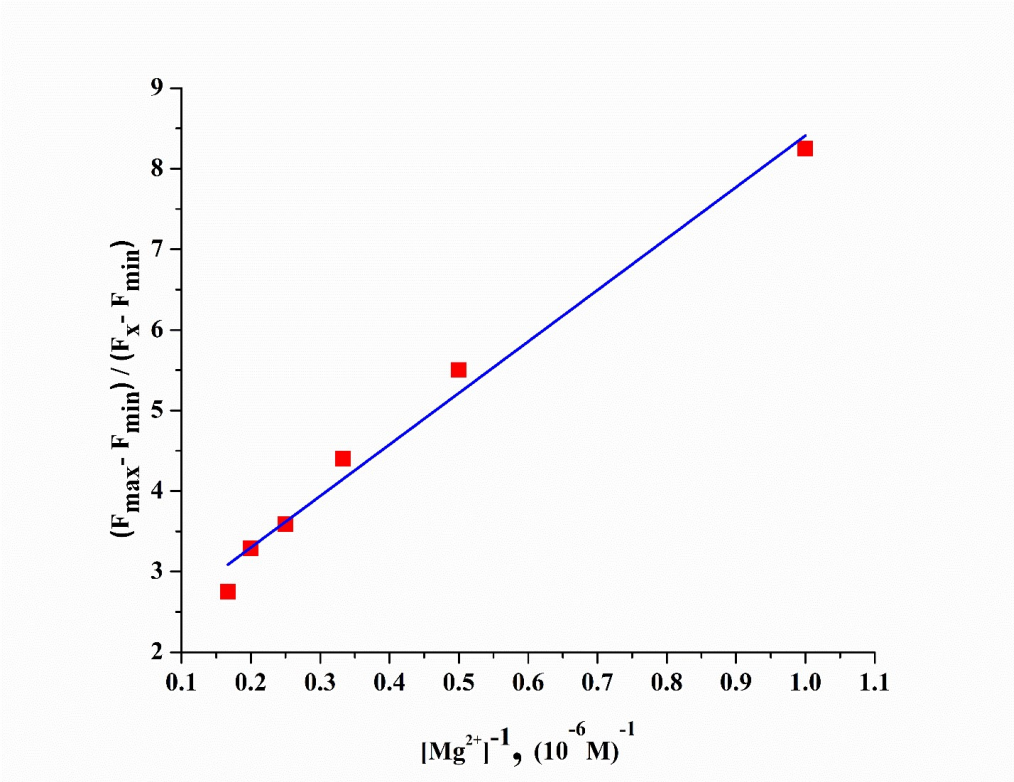

Fig. S12 Determination of displacement binding constant of **[Fe(III)-TNESAL]** for Mg^{2+}.

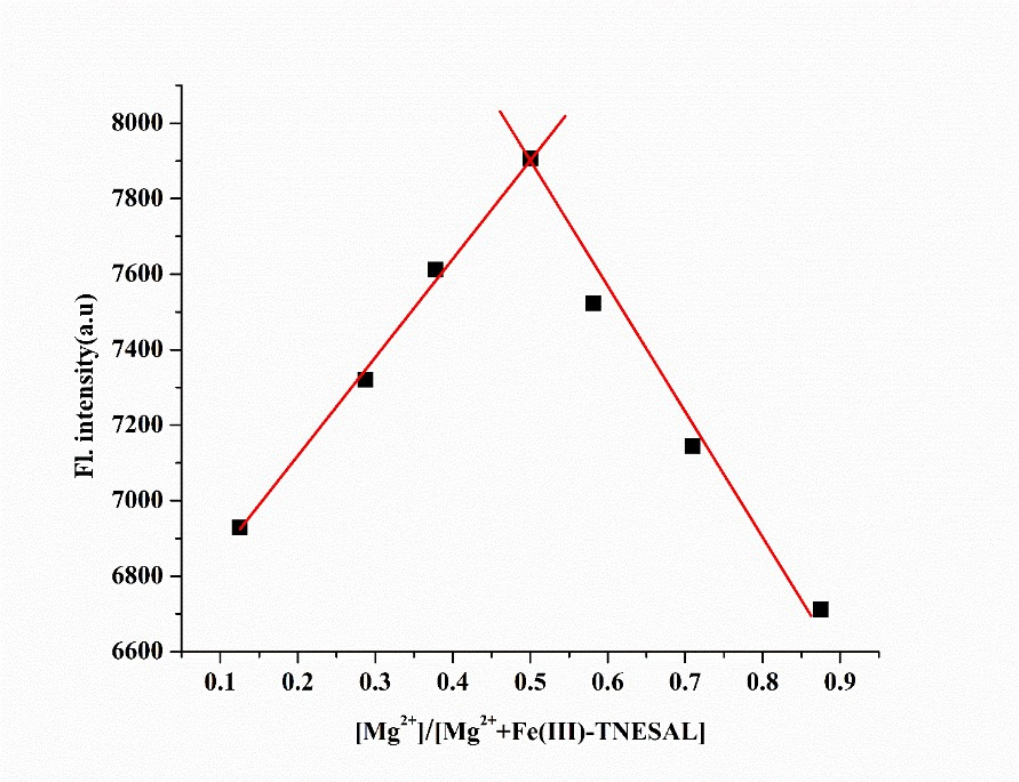

Fig. S13 Job's plot for determination of stoichiometry of interaction between [**Fe(III)-TNESAL**] complex and Mg^{2+}.

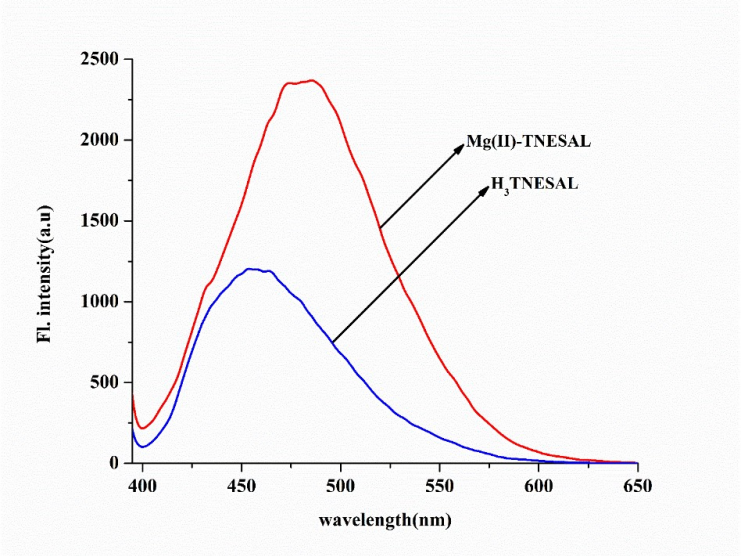

Fig. S14 Emission spectra of **[Mg(II)-TNESAL]** complex (λ_{em}, 488 nm) and **H_3TNESAL** (λ_{em}, 454 nm)

Table S1 Selected bond angles and lengths of **[Fe(III)-TNESAL]** complex

Atoms	Angle	Atoms	Distance
O1 Fe1 O2	93.01(6)	Fe1 O1	1.9457(14)
O1 Fe1 O3	93.03(6)	Fe1 O2	1.9476(14)
O2 Fe1 O3	92.81(6)	Fe1 O3	1.9526(14)
O1 Fe1 N1	177.13(6)	Fe1 N1	2.1761(17)
O2 Fe1 N1	86.21(6)	Fe1 N4	2.1788(17)
O3 Fe1 N1	84.25(6)	Fe1 N3	2.1827(17)
O1 Fe1 N4	84.23(6)	C1 N2	1.447(3)
O2 Fe1 N4	177.06(6)	C1 C2	1.522(3)
O3 Fe1 N4	86.33(6)	O1 C31	1.305(2)
N1 Fe1 N4	96.49(6)	N1 C7	1.299(3)
O1 Fe1 N3	86.22(6)	N1 C6	1.478(3)
O2 Fe1 N3	84.51(6)	N2 C5	1.442(3)
O3 Fe1 N3	177.17(6)	N2 C3	1.442(3)
N1 Fe1 N3	96.45(6)	O2 C13	1.309(2)
N4 Fe1 N3	96.30(6)	C2 N3	1.480(3)
N2 C1 C2	111.4(2)	O3 C24	1.304(2)
C31 O1 Fe1	133.80(13)	C3 C4	1.518(3)
C7 N1 C6	115.22(18)	N3 C25	1.296(3)
C7 N1 Fe1	123.73(14)	N4 C16	1.290(3)
C6 N1 Fe1	120.09(14)	N4 C4	1.485(3)
C5 N2 C3	118.0(2)	O4 C30	1.373(3)
C5 N2 C1	117.8(2)	O4 C32	1.403(4)
C3 N2 C1	117.5(2)	O5 C21	1.373(3)
C13 O2 Fe1	133.87(13)	O5 C22	1.396(3)
N3 C2 C1	109.37(19)	C5 C6	1.522(3)
C24 O3 Fe1	133.65(13)	C9 C10	1.356(4)
N2 C3 C4	111.6(2)	C9 C8	1.409(3)
C25 N3 C2	115.14(18)	C8 C13	1.409(3)
C25 N3 Fe1	123.67(14)	C8 C7	1.442(3)
C2 N3 Fe1	120.27(14)	O6 C12	1.370(3)
C16 N4 C4	115.35(19)	O6 C14	1.396(4)
C16 N4 Fe1	123.67(14)	C10 C11	1.380(4)
C4 N4 Fe1	120.05(14)	C11 C12	1.391(4)
C30 O4 C32	115.5(2)	C12 C13	1.420(3)
N4 C4 C3	109.40(19)	C14 C15	1.464(5)
C21 O5 C22	115.3(2)	C16 C17	1.448(3)
N2 C5 C6	111.8(2)	C18 C19	1.361(4)
C10 C9 C8	121.9(2)	C18 C17	1.410(3)
C13 C8 C9	119.8(2)	C19 C20	1.382(4)
C13 C8 C7	123.26(19)	C20 C21	1.390(3)
C9 C8 C7	116.9(2)	C21 C24	1.425(3)
N1 C7 C8	127.05(19)	C22 C23	1.468(5)

C12 O6 C14	115.2(2)	C24 C17	1.410(3)
N1 C6 C5	109.35(19)	C25 C26	1.439(3)
C9 C10 C11	119.3(2)	C26 C31	1.411(3)
C10 C11 C12	121.0(2)	C26 C27	1.415(3)
O6 C12 C11	118.6(2)	C27 C28	1.354(4)
O6 C12 C13	120.4(2)	C28 C29	1.385(4)
C11 C12 C13	120.7(2)	C29 C30	1.391(3)
O2 C13 C8	123.50(18)	C30 C31	1.421(3)
O2 C13 C12	119.18(19)	C32 C33	1.463(5)
C8 C13 C12	117.27(19)		
O6 C14 C15	111.6(3)		
N4 C16 C17	127.15(19)		
C19 C18 C17	121.7(2)		
C18 C19 C20	119.5(2)		
C19 C20 C21	121.0(2)		
O5 C21 C20	118.7(2)		
O5 C21 C24	120.6(2)		
C20 C21 C24	120.5(2)		
O5 C22 C23	111.5(3)		
O3 C24 C17	123.54(18)		
O3 C24 C21	118.95(19)		
C17 C24 C21	117.47(19)		
N3 C25 C26	126.96(19)		
C31 C26 C27	120.0(2)		
C31 C26 C25	123.49(18)		
C27 C26 C25	116.5(2)		
C28 C27 C26	121.5(2)		
C27 C28 C29	119.5(2)		
C28 C29 C30	121.1(2)		
O4 C30 C29	119.0(2)		
O4 C30 C31	120.2(2)		
C29 C30 C31	120.6(2)		
O1 C31 C26	123.51(17)		
O1 C31 C30	119.14(19)		
C26 C31 C30	117.29(19)		
O4 C32 C33	111.5(3)		
C18 C17 C24	119.8(2)		
C18 C17 C16	116.9(2)		
C24 C17 C16	123.28(18)		

Table S2 Comparison with pioneering Mg^{2+} selective probes available in literature

Sl No	Probe	Media	Sensing type	Mechanism	LOD	Ref.
1	$Ce_2(C_{17}H_{14}N_4O_4)_3 \cdot 3CH_3OH \cdot 6H_2O$ $Ce_2(C_{25}H_{18}N_4O_4)_3 \cdot 3H_2O \cdot CH_3OH$	DMF-CH_3CN (1 : 99, v/v)	Turn on	PET operates between amide unit and Ce^{3+} chelated unit	-	49
2	$Ce_2(C_{30}H_{24}N_4O_6)_3 \cdot 3C_3H_7ON$ $Ce_2(C_{48}H_{40}N_4O_6)_3NO_3 \cdot 3C_3H_7ON$	DMF-CH_3CN (1 : 9, v/v)	Turn on	Impeding the PET processes	-	50
3	$C_{102}H_{65}Eu_4N_9O_{46.5}$	EtOH	Turn on	Donor-acceptor electron transfer	1.53×10^{-10} M	51
4	$C_{20}H_{16}N_2O_2$ $C_{22}H_{20}N_2O_4$ $C_{20}H_{16}N_2O_4$	DMF	Turn on	Restriction of -CH=N isomerisation and enhanced rigidity	10^{-7} M	52
5	$C_{19}H_{17}N_2O_5$	DMSO/ H_2O (7 : 3, v/v, 0.01 M HEPES, pH, 8.5)	Turn on	Inhibition of ESIPT	9.2×10^{-10} M	53
6	$C_{18}H_{14}N_2O_2$	CH_3CN/H_2O (9 : 1 v/v) in HEPES buffer, pH 7.2	Turn on	Complex formation between the probe and Mg^{2+}	2.04 nM	54
7	Fe_3O_4/RhB@Al-MOFs	Water	Turn on	Energy transfer between Mg^{2+} and Al-MOFs	8×10^{-7}M	55
8	$C_{11}H_8O_4$	CH_3OH	Turn on	Complex formation between the probe and Mg^{2+}	0.43 μM	56
9	$C_{44}H_{34}N_4O_2$	DMSO/ DMF/THF	Turn on	Complex formation between the probe and Mg^{2+}	10^{-6}M	57
10	$C_{28}H_{28}N_2O_2S_2$	H_2O- DMF (9.9/ 0.1)	Turn on	Complex formation inhibits the PET process from nitrogen donor of the receptor to the naphthyl rings is restrained	10^{-8} M	58
11	$C_{16}H_{12}N_2O_3$	CH_3CN/H_2O (8:2, v/v)	Turn on	Due to complex formation	0.09 μM	59
12	$C_7H_4Cl_2O_2$	Ethanol-HEPES buffer (95:5, v/v, 0.05 M, pH, 7.0)	Turn on	CHEF	2.89×10^{-7} M	60
13	Tryptophan functionalized AuNPs	Aqueous	Turn on	Complex formation	0.2 μmol L^{-1}	61
14	MagFRET-1 (Genetically Encoded)	150 mM HEPES (pH 7.1), 100 mM	Turn on	Ligand-induced folding of intrinsically-	-	62

		NaCl, 10% (v/v) glycerol		disordered proteins		
15	$C_{21}H_{17}N_4O_3$	HEPES buffered CH_3CN/H_2O (8:2, v/v, pH, 7.0)	Turn on	Formation of a 1:1 host/ guest complex	3.2-100 μM	63
16	$C_{22}H_{22}N_2O_4$	MeOH-H_2O	Turn on	Arresting -CH=N bond isomerization and inhibition of the ESIPT process	-	64
17	$C_{37}H_{34}N_4O_3$	CH_3CN	Turn on	Formation of 1:1 ligand–metal complexes and inhibition PET process	1.44×10^{-6}M	65
18	N-doped carbon dots (NCDs) using 4-hydroxybenzaldehyde and 1, 2, 4, 5-benzenetetramine tetrahydrochloride	Aqueous	Turn on	Chelation	60 μM	66
19	$C_{22}H_{13}ON_5$	EtOH	Turn on	CHEF	3.3×10^{-8} M	67
20	$C_{16}H_{10}N_2OS$	DMSO-HEPES buffer (pH = 7.0, 9:1 (v/v))	Turn on	CHEF	0.142 μM	68
21	$C_{15}H_9N_3O_6$ and $C_{15}H_9BrN_2O_4$	CH_3CN	Turn on	LMCT	2.56×10^{-6} and 1.28×10^{-6} M	69
22	$C_{33}H_{39}FeN_4O_6$	DMF-water, (3 : 1, v/v, 1 M HEPES buffer, pH 8.1)	Turn on	Metal ion displacement	7.66×10^{-9}M	**Present work**